Adaptation of Energy Dissipation in a Mechanical Metastable Module Excited Near Resonance

N. Kidambi
Department of Mechanical Engineering,
University of Michigan,
Ann Arbor, MI 48109-2125

R. L. Harne[1,2]
Department of Mechanical Engineering,
University of Michigan,
Ann Arbor, MI 48109-2125
e-mail: rharne@umich.edu

K. W. Wang
Department of Mechanical Engineering,
University of Michigan,
Ann Arbor, MI 48109-2125

Recent studies have demonstrated that the energetic vibrations of strategically designed negative stiffness inclusions may lead to large and adaptable damping in structural/material systems. Many researchers examine these features using models of bistable elements. From the viewpoint of system integration, bistable, negative stiffness elements often interface with positive stiffness elastic members. Under such conditions, the structural/material system may exhibit coexisting metastable states. In other words, the macroscopic displacement/strain remains fixed while the reaction force may vary due to internal change, similar to a phase transition. This coexistence of metastable states is not manifested in an individual (stand-alone) bistable element. Although the static and low frequency linear dynamics of structural/material systems possessing coexisting metastable states have been explored, much remains to be understood regarding the dynamics and energy dissipation characteristics of such systems when excited near resonance, where nonlinear dynamics are more easily activated and damping design is of greater importance. Thus, to effectively elucidate the enhanced versatility of damping properties afforded by exploiting negative stiffness inclusions in structural/material systems, this research investigates a mechanical module which leverages a coexistence of metastable states: an archetypal building block for system assembly. The studies employ analytical, numerical, and experimental findings to probe how near-resonant excitation can trigger multiple dynamic states, each resulting in distinct energy dissipation features. It is shown that, for lightly damped metastable mechanical modules, the effective energy dissipation may be varied across orders of magnitude via tailoring design and excitation parameters.
[DOI: 10.1115/1.4031411]

1 Introduction and Research Goals

Many modern engineering applications would greatly benefit from the availability of structural and material systems demonstrating large and adaptable energy dissipation. For example, a structure may call for large damping to preserve system integrity under sudden, extreme loading events, whereas a more easily excited vibrational response may be preferred to effectively transmit dynamic signals for system identification or damage detection. In recent years, researchers have investigated the use of negative stiffness inclusions in structures and materials in order to achieve large and adaptable damping properties. In particular, bistable elements exhibiting negative stiffness have shown potential for significant and tunable damping, primarily due to energetic transitions between stable equilibrium positions, a phenomenon termed *snap-through*.

The physical properties of composite materials fabricated with negative stiffness inclusions within a positive stiffness host structure have been of particular research interest. Lakes [1] and Wang and Lakes [2] demonstrated large macroscopic energy dissipation when the temperature of such a composite was held within a critical regime; outside of this temperature range, material damping was reduced. Klatt and Haberman [3] developed a multiscale model to understand the variation in effective macroscopic properties due to tailoring microstructural composition of positive and negative stiffness constituents. Kochmann [4] derived stability criteria for viscoelastic composite media having a non-positive-definite (negative) stiffness phase, thereby providing guidelines for material selection and processing to obtain extreme damping properties under conditions of low frequency linear oscillations.

Barbarino et al. [5] numerically quantified the energy dissipation capabilities of an individual, harmonically excited bistable von Mises truss, demonstrating large change in damping as device configuration and excitation frequency were varied. Johnson et al. [6] explored damping enhancement and adaptation that was facilitated by a compressed spring–mass bistable device, and evaluated the influence of initial conditions on power dissipation performance. Using an additive manufacturing technique, Kashdan et al. [7] fabricated a fully nylon-based vibration isolator composed from an axially compressed beam connected in series with a linear spring to investigate the transmissibility and damping tunability enabled by tailoring the precompression distance while the overall vibration levels were held within a linear regime, while Fulcher et al. [8] assessed the accuracy of an analytical model toward predicting the isolation performance of comparable device platforms. Dong and Lakes [9] examined parallel column systems subjected to low frequency harmonic loads, showing that weaker columns of the system would buckle (become bistable) to effect large damping. Nadkarni et al. [10] discovered three dynamic regimes of wave propagation in a chain of bistable elements, while Cohen and Givli [11] explored a biologically inspired design consisting of series-connected bistable/bilinear elements that might enhance shock absorption capacity by a "reversible rupture" phenomenon.

The previous works conclusively find that negative stiffness inclusions (i.e., bistable devices/elements) can yield significant energy dissipation under strategic situations. From the viewpoint of system integration, bistable, negative stiffness elements often interface with positive stiffness elastic members. A fundamental, one-dimensional, and unit-level model of the integration may be of bistable and linear (positive stiffness) springs in series [4,12], which exhibits very different properties compared to an individual bistable element. To clarify the considerable distinctions, the inset of Fig. 1(*a*) shows the archetypal, one-dimensional mechanical module examined in this research: a bistable spring (axially-compressed rigid bars joined at a central pivot) connected in series

[1]Corresponding author.
[2]Current affiliation: Department of Mechanical and Aerospace Engineering, The Ohio State University, Columbus, OH 43210; e-mail: harne.3@osu.edu.
Contributed by the Technical Committee on Vibration and Sound of ASME for publication in the Journal of Vibration and Acoustics. Manuscript received February 18, 2015; final manuscript received June 26, 2015; published online October 8, 2015. Assoc. Editor: Paul C.-P. Chao.

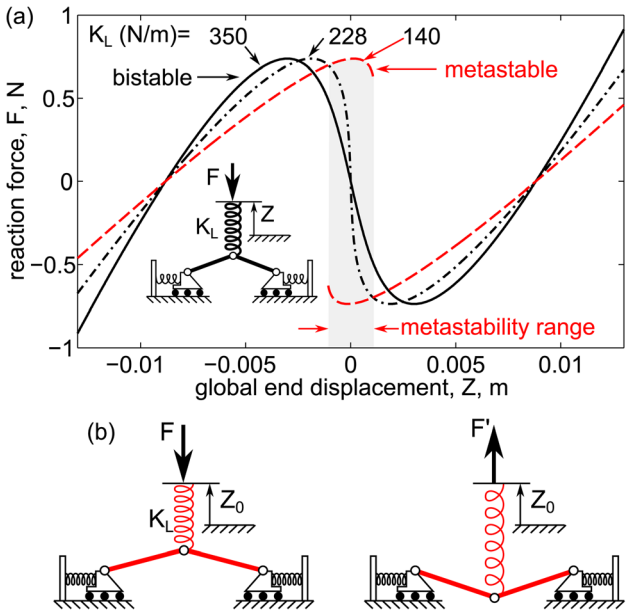

Fig. 1 (*a*) Inset: Schematic of the mechanical module that integrates bistable and liner springs in series. Reaction force, *F*, of mechanical module acted upon by a global end displacement, *Z*, for three linear spring stiffnesses K_L. (*b*) For sufficiently small linear spring stiffness, the system exhibits coexisting metastable states evidenced by more than one reaction force for one end displacement.

with a linear spring with stiffness coefficient K_L. When the module is constrained by a static, global end displacement Z at the free end of the linear spring, the qualitative character of the reaction force F evaluated at the end will significantly vary based upon the relative amplitude of the stiffnesses between the bistable and linear spring constituents.

For example, the black solid curve in Fig. 1(*a*) shows the case for which the linear spring is very stiff compared to the bistable spring. Since the "weakest link" of springs in series governs the upper bound on the effective stiffness, a macroscopic observation taken from the end displacement is that this module is effectively bistable, and therefore exhibits only one potential reaction force as the global end displacement varies. As the linear spring stiffness K_L is reduced, a dramatic change in mechanical properties occurs. At a critical reduction of the linear spring stiffness, a vertical tangency appears in the force–displacement profile [13], such as that shown for the dashed–dotted curve in Fig. 1(*a*). Thus, the continued reduction in the linear spring stiffness leads to two *coexistent metastable states*, shown by the dashed curves in Fig. 1(*a*). In this research, a module having multiple coexisting metastable states over a given range of displacements is referred to as a *metastable module*. The coexisting states are illustrated in Fig. 1(*b*) where for one prescribed end displacement Z_0 there are two unique static internal configurations that induce unique reaction forces F and F'. For the mechanical system employed in this study, the *metastability range* is defined as the extent of displacements across which the module exhibits a coexistence of metastable states.

Based on the above arguments, integrating negative stiffness (bistable) inclusions or devices into structural/material systems to effect large and adaptable damping may commonly result in a system possessing coexisting metastable states, and the unit-level module of such a phenomenon serves as a suitable model to explore the global features [4,12]. While such metastable modules have been examined for their static and subresonant low frequency dynamic properties [1–4], to date much remains to be understood regarding the dynamics and energy dissipation characteristics of metastable modules when excited near resonance, i.e., at frequencies close to the linearized resonances of the locally stable states. Such scenarios are particularly important since near-resonant excitations are substantially more influential on the activation of large amplitude snap-through dynamics in individual bistable devices [14] and damping change has greater impact around system resonances.

The goals of this research are to investigate the dynamic characteristics of a metastable module when excited near resonance, and to identify how the various dynamic states may be leveraged to achieve large and adaptable energy dissipation properties at the unit module level. The study considers an archetypal mechanical metastable module to realize the essential components of negative and positive stiffness members configured in series. Sections 2–7 introduce the experimental platform and corresponding one degree-of-freedom (DOF) model of the metastable module, then present analytical, numerical, and experimental investigations to evaluate the effects of excitation parameters on the energy dissipation properties effected via near-resonant excitation.

2 Experimental Metastable Module

The experimental system studied in this research is depicted in Fig. 2, and represents the essential constituents required to closely examine the dynamics of an individual metastable module. A polycarbonate base (label a) supports a suspension system consisting of a pair of parallel, thin spring steel beams (label b) clamped at the ends. At the center of each spring steel beam suspension is a miniature ball bearing that serves as a mount for a rigid, rotating arm (label c). The other ends of the arms are pinned together at a center point between the suspensions using similar bearings in the arms and a shared axle. The net length of the two rotating arms is greater than the distance between the suspension system ends and thus the subsystem is bistable. Due to the compliance provided by the suspensions, the rigid arms may rotate between the two stable equilibria. The configuration used throughout experimentation is designed such that the two stable equilibria of the bistable constituent are at ± 10 deg with respect to a line normal to the suspension beams. These prior elements represent the bistable spring of the metastable module. A pair of linear tension springs (label d) connects the shared axle that joins the two rotating arms to bolts protruding from a rigid U-channel beam (label e). The tension springs are always extended from the relaxed lengths to avoid the possibility of spring buckling. The U-channel beam, to which the tension springs are connected, is fixed to a controlled electrodynamic shaker (APS Dynamics 400, label f), which is the global

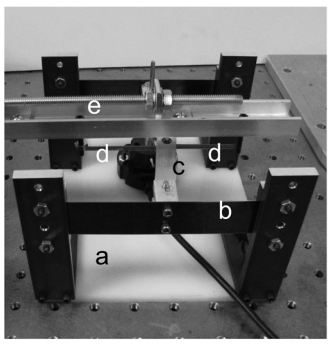

(a) polycarbonate base
(b) flexible spring steel beams
(c) rotating aluminum arms
(d) linear extension springs
(e) U-channel
(f) electrodynamic shaker
(g) Hall effect sensor

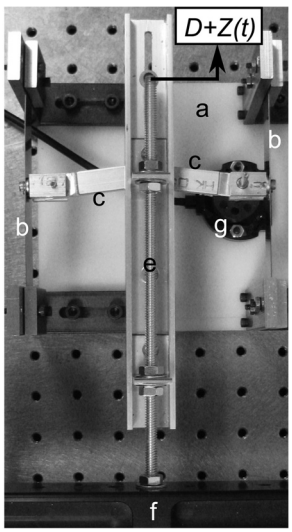

Fig. 2 Experimental metastable module and experimentation components. The configuration used throughout experimentation is such that the two stable equilibria of the bistable constituent are at $\theta = \pm 10$ deg.

end displacement (excitation) for the metastable module. The bolts connecting the U-channel to the springs may be moved to generate a static offset to the excitation. Experiments verified that the U-channel beam was sufficiently rigid to eliminate resonant dynamics of the U-channel in the frequencies of interest in this research. The energy dissipation mechanisms present in the system are primarily the result of viscous damping in the deformation of the springs and suspension beams, as well as the unavoidable friction in the bearings. To monitor the excited dynamics of the metastable module, the rotation of the rigid arms is measured using a Hall effect sensor (Novotechnik RFC-4801, label g) attached to the pinned axle that connects one arm to a suspension, as shown in Fig. 2. Additionally, the input shaker acceleration is monitored by an accelerometer (PCB 352 C33).

3 Model Formulation and Governing Equation

The experimental module shown in Fig. 2 is modeled using the schematic of Fig. 3, and the governing equation of motion is derived using energy principles. The mass taken into consideration in this study consists only of the rigid rotating arms, while the masses of the other components of the module relative to the arms are assumed to be negligible. The total kinetic energy of the module may then be derived as

$$T = 2\left[\frac{1}{2}\left(I_p + M\frac{L^2}{4}\right)\right]\dot{\theta}^2 \tag{1}$$

The rotation of both arms is expressed using one common angular displacement $\theta(t)$, M is the mass of each rotating arm of length L, and I_p is the moment of inertia of each rigid arm about an axis through its center of mass, perpendicular to the plane shown in Fig. 3. The parallel axis theorem is applied to obtain the moment of inertia of the rigid arm about its pinned end. The potential energy stored in the suspension beams may be written as

$$U_1 = 2\frac{192\text{EI}}{L_s^2}\left[1 - \theta\sin(\theta) - \cos(\theta) + \frac{1}{2}\theta^2\cos(\theta_0)\right] \tag{2}$$

where E is the Young's modulus of the suspension beam, I is the area moment of inertia about the neutral axis of bending, L_s is the length from clamp to clamp of each suspension, and θ_0 is the angular position of the arms that results in the absence of the connection to the linear springs. The term $192\text{EI}/L_s^3$ is the effective, one-dimensional spring stiffness of a clamped–clamped beam with an applied load at the center point [15]. The potential energy stored in the linear springs is

$$U_2 = K_L[Z + D - L\sin(\theta)]^2 \tag{3}$$

where tension spring stiffness is K_L, and D refers to a static offset of the periodic excitation Z from the neutral position of the bistable device. In other words, a nonzero offset D biases the system toward one of the two potential wells. The offset is adjusted experimentally by changing the pretension on one of the linear springs. Dissipation is approximated by a viscous damping force proportional to the angular velocity of the rigid, rotating arms according to the coefficient B, whose value is determined by fitting numerical results to experimentally measured data of the free decay response. Lagrange's equations are used to yield the governing equation of motion for the rigid arm rotation θ in consequence to certain end displacement motions Z.

$$\left(\frac{ML^2}{2} + 2I_p\right)\ddot{\theta} + B\dot{\theta} + 2K_L L^2\sin(\theta)\cos(\theta) - \frac{384\text{EI}}{L_s^2}\theta\left[\cos(\theta) - \cos(\theta_0)\right] - 2K_L L\ (Z + D)\ \cos(\theta) = 0 \tag{4}$$

In this study, the global energy dissipation of the metastable module due to harmonic excitations of the end displacement, $Z(t) = Z_0\cos\Omega t$, is quantified by computing the area enclosed in the hysteresis loops of reaction force and end displacement. The reaction force due to the deflection of the linear springs is defined in Eq. (5). In addition to the apparent spring force contribution, the reaction force also reflects inertial and energy dissipation phenomena due to the influences of the rotations θ of the internal moving arms.

$$F(t) = 2K_L[Z + D - L\sin(\theta)] \tag{5}$$

4 Model Transformation and Equivalent Governing Equation

Equation (4) may be directly integrated via numerical methods to predict the response and energy dissipation properties due to a particular selection of design and excitation parameters for the metastable module. On the other hand, to obtain more comprehensive insights on the potential dynamic behaviors, an approximate analytical strategy to solve the governing equation (4) is undertaken in this study. As a first step toward application of an approximate solution, the restoring forces in Eq. (4) are expanded via a Taylor series around $\theta = 0$, retaining terms up to the third-order.

$$\left(\frac{ML^2}{2} + 2I_p\right)\ddot{\theta} + B\dot{\theta} - \frac{384\text{EI}}{L_s^2}[1 - \cos(\theta_0)]\theta + [K_L L(Z + D)]\theta^2 + \left(-\frac{4}{3}K_L L^2 + \frac{192\text{EI}}{L_s^2}\right)\theta^3 - 2K_L L(Z + D - L\theta) = 0 \tag{6}$$

By performing a coordinate transformation around a stable angular equilibrium θ_0 of the internal bistable element when disconnected from the linear spring [16], and by applying the arc length relationship ($x = L\theta$) to relate the displacement of the center axle joining the rigid arms x to the angular rotation of the arms θ, the following governing equation may be obtained:

$$m\ddot{x} + b\dot{x} + k_1 x + k_2 x^2 + k_3 x^3 - k_L(z + d - x) = 0 \tag{7}$$

where m is the lumped internal mass, and k_1, k_2, and k_3 are the linear, quadratic, and cubic stiffness coefficients, respectively. Figure 4 shows a schematic representation of the metastable

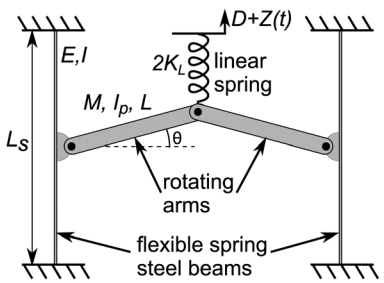

Fig. 3 Schematic of the experimental metastable module

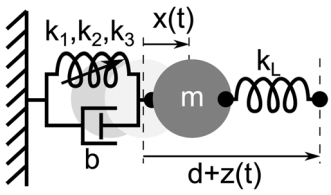

Fig. 4 Schematic of the transformed model formulation of the metastable module

module using the parameters expressed in Eq. (7). With the restoring forces of the module approximated by the power series in terms of the displacement x, the governing equation (7) may be approximately solved using a variety of assumed solution techniques to predict the steady-state behaviors [17].

4.1 Approximate Solution to the Transformed Model. In this study, the solution to Eq. (7) is approximated using a fundamental Fourier series expansion

$$x(t) = f(t) + g(t)\sin(\omega t) + h(t)\cos(\omega t) \tag{8}$$

where the coefficients f, g, and h are assumed to slowly vary in time with respect to the primary period of oscillation. The excitation z considered here is a harmonic in frequency ω and amplitude z_0

$$z(t) = z_0\cos(\omega t) \tag{9}$$

Substituting Eqs. (8) and (9) into Eq. (7), assuming slowly varying harmonic coefficients such that $\dot{f}(t) = \dot{g}(t) = \dot{h}(t) = 0$, and retaining only those harmonic terms proportional to the assumed solution expansion, the following equations are obtained via balancing the coefficients of the constant, sine, and cosine terms, respectively.

$$-b\dot{f} = k_1 f + k_2 f^2 + \frac{k_2}{2}r^2 + k_3\left(\frac{3}{2}fr^2 + f^3\right) + k_L(f-d) \tag{10a}$$

$$2m\omega\dot{h} - b\dot{g} = k_1 g + 2k_2 gf + k_3\left(\frac{3}{4}gr^2 + 3gf^2\right) + k_L g - mg\omega^2 - bh\omega \tag{10b}$$

$$-2m\omega\dot{g} - b\dot{h} = k_1 h + 2k_2 hf + k_3\left(\frac{3}{4}hr^2 + 3hf^2\right) + k_L h - k_L z_0 - mh\omega^2 + bg\omega \tag{10c}$$

The amplitude of the motion of x is expressed by $r = [g^2 + h^2]^{1/2}$. Assuming steady-state response, which implies that $\dot{f}(t) = \dot{g}(t) = \dot{h}(t) = 0$, Eqs. (10*a*)–(10*c*) are combined to yield a system of two equations for r and f, representing response amplitude and offset, respectively.

$$k_3 f^3 + k_2 f^2 + \left(k_1 + k_L + \frac{3}{2}k_3 r^2\right)f + \frac{1}{2}k_2 r^2 - dk_L = 0 \tag{11a}$$

$$\frac{9}{16}k_3 r^6 + \frac{3}{2}k_3\left(-m\omega^2 + k_1 + k_L + 3k_3 f^2 + 2k_2 f\right)r^4 + \left[\left(-m\omega^2 + k_1 + k_L + 3k_3 f^2 + 2k_2 f\right)^2 + b^2\omega^2\right]r^2 - k_L^2 z_0^2 = 0 \tag{11b}$$

Equations (11*a*) and (11*b*) are nonlinearly coupled and must be solved numerically, although the solutions are an analytical approximation to the steady-state dynamics of the metastable module. The solutions must then be evaluated for stability. From Eq. (10), the response coefficients may be expressed using

$$g = -\frac{bk_L z_0\omega}{\Gamma^2 + b^2\omega^2} \tag{12a}$$

$$h = -\frac{k_L z_0}{\Gamma^2 + b^2\omega^2} \tag{12b}$$

where

$$\Gamma = k_1 + 2k_2 f - m\omega^2 + k_3\left(3f^2 + \frac{3}{4}r^2\right) + k_L \tag{13}$$

Equation (10) is then expressed in a conventional form using $\mathbf{x} = [f, g, h]^{\mathrm{T}}$

$$\mathbf{Q}\dot{\mathbf{x}} = \mathbf{P}(\mathbf{x}) \tag{14}$$

where $\mathbf{Q}$ and $\mathbf{P}$ are determined by consideration of Eq. (10). Then, linearizing the system around one of the fixed points $\mathbf{x}^* = [f, g, h]^{\mathrm{T}}$ obtained from solving Eqs. (11) and (12), the stability of the fixed point is found by evaluating the eigenvalues of the Jacobian matrix of the linearized system, where the Jacobian is $\mathbf{J} = \mathbf{D}_{\mathbf{x}}(\mathbf{Q}^{-1}\mathbf{P}(\mathbf{x}))_{\mathbf{x}^*}$. The fixed point solution is stable if all eigenvalues of the Jacobian have negative real parts.

In this study, steady-state results of the amplitude r are qualitatively compared to the experimentally measured results of angular rotation magnitude $|\theta|$. Only the stable results of the analytically approximated amplitude r are presented. Additionally, for a quantitatively meaningful comparison, Eq. (4) is numerically integrated, and the dynamic reaction force $F(t)$ from Eq. (5) is compared to the corresponding measured result conducted using common system parameters.

5 Excitation Frequency Influence on Energy Dissipation

It is well known that structures containing buckled members may more readily exhibit strongly nonlinear dynamics when excited near resonance [14] and this feature has indeed been exploited to achieve high and adaptable damping using an individual bistable oscillator [6]. But the ways in which such an excitation comparably influences the dynamics of metastable modules, like the one studied here with bistable-linear spring integrations, remain poorly understood.

To investigate the frequency dependence of the near-resonant harmonic excitation, experimental excitation frequency sweeps are performed at fixed amplitude using very slow sweep rates of $\pm$ 0.05 Hz/s to ensure that steady-state responses are correctly identified and that all potential dynamic states are realized by sweeping both up and down in frequency. First, the examinations consider the case in which the offset parameter D is set such that the mean value of the harmonic excitation corresponds to the central unstable equilibrium position of the internal bistable device of the metastable module. For the offset D satisfying the condition described above, the linear spring stiffness K_L is selected such that the module exhibits coexistent metastable states. Experimental and analytical model parameters are presented in Tables 1 and 2, respectively. Analytical model parameters are chosen to facilitate a qualitative comparison between the experimental measurements and analytical model predictions. At this phase of research development, the aim of the analytical model is to demonstrate an ability to predict the overall characteristics of the strongly nonlinear experimental system dynamics as excitation parameters are varied. Once the analytical model is verified qualitatively, future efforts will pursue quantitative validations of the results using appropriate nondimensional parameters derived from a transformation of Eq. (6) to Eq. (7).

Figure 5 presents (*a*) experimental and (*b*) analytical results of the rigid arm rotation and displacement amplitudes, respectively.

Table 1 Experimental system parameters used in numerical simulations

M (g)	I_P (kg/m^2)	L (cm)	E (GPa)	I (m^4)
12	1.05	5.08	180	5.46×10^{-15}
L_s (cm)	θ_0 (deg)	K_L (N·m^{-1})	B (N·s·m^{-1})	
10.02	$\pm$10	84	1.5×10^{-4}	

Table 2 Analytical model parameters

m (kg)	k_1 (N·m^{-1})	k_2 (N·m^{-2})	k_3 (N·m^{-3})	k_L (N·m^{-1})	b (N·s·m^{-1})
1	2	−3	1	0.5	0.05

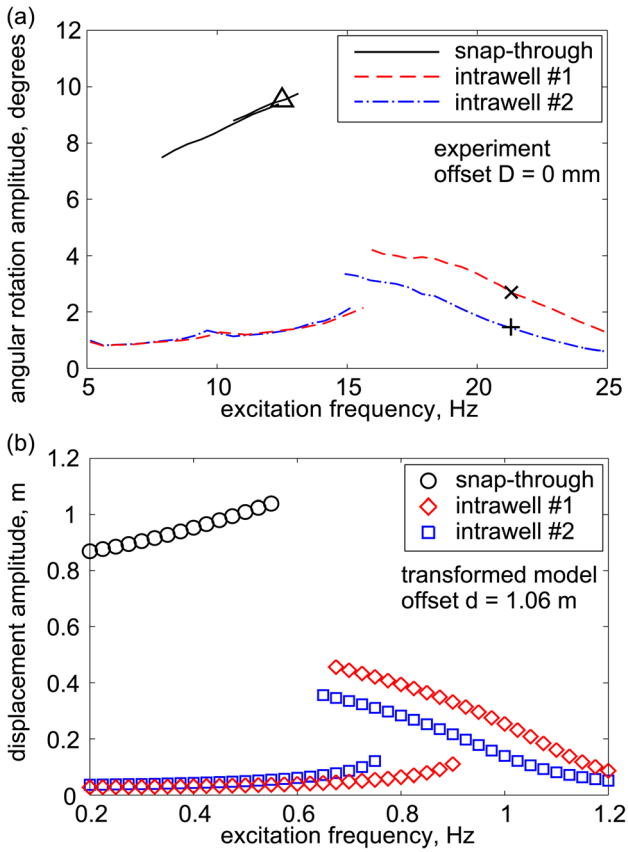

Fig. 5 (*a*) Experimentally measured angular rotation amplitude of the rigid arms and (*b*) analytical predictions of the displacement amplitude as the excitation frequency is varied. In (*a*), three data points are provided as reference to results shown in Fig. 6.

In the experiments, the harmonic excitation frequency varies from 5 to 25 Hz with a constant excitation amplitude $Z_0 = 300\,\mu$m. Statically stable equilibria of the bistable constituent of the experimental module are at angular positions ± 10 deg. The transformed analytical model, Eq. (7), is evaluated between normalized frequencies of 0.2 Hz and 1.2 Hz, with excitation amplitude $z_0 = 0.1$ m. Both the experimental and analytical results reveal two distinct dynamic regimes: intrawell and interwell. *Intrawell* responses oscillate around a statically stable equilibrium. As described using the illustration of Fig. 1, for some configurations of the module, the system possesses two local wells of potential energy such that it exhibits coexistence of metastable states for a prescribed end displacement Z. For clarity, these two local wells are referred to throughout the rest of this study as *well #1* and *well #2*, and intrawell responses observed in these potential wells are labeled in all figures as *intrawell #1*, and *intrawell #2*, respectively. Interwell (i.e., *snap-through*) responses are characterized by displacements which cross the unstable equilibrium of the internal bistable constituent. These response behaviors are exhibited by individual bistable oscillators [18], and are observed here due to the internal bistable element within the metastable module and the corresponding module design and excitation parameters. For the excitation offset $D = 0$ mm, the metastable module displays two statically stable equilibria. Since the excitation amplitude Z_0 is sufficiently small, two distinct intrawell-type dynamics are activated, as shown in Fig. 5(*a*) by the dashed and dashed–dotted curves. This is a unique coexistence of dynamics not manifest in an individual, displacement-driven bistable device. For certain excitation frequencies, namely those close to 15 Hz, two different intrawell responses are observed for each of the intrawell-type behaviors: *low* and *high amplitude* intrawell. In particular, these two responses are realized due to the near-resonant excitation frequencies. The continuous snap-through oscillations, shown by a solid line in Fig. 5(*a*), are observed at excitation frequencies between 8 Hz and 14 Hz, with much greater response amplitudes than either of the intrawell oscillations. Due to the differences in the angular rotation amplitudes among each dynamic type across the near-resonant frequencies explored here, the kinetic energies of the dynamic regimes are distinct. Because the metastable module possesses internal damping mechanisms, a wide variation of energy dissipation capabilities is correspondingly achieved, and is shown to be governed by the harmonic excitation frequency in this case.

The excitation offset position $D = 0$ mm is presumed to be centered on the unstable equilibrium of the internal bistable element. Hence, an ideal, symmetric, module should exhibit identical intrawell responses. Yet, the different response amplitudes, particularly for the high amplitude intrawell responses found at frequencies greater than 15 Hz, indicate that the experimental metastable module is slightly asymmetric. Note that due to the coordinate transformation performed to reduce Eq. (6) to the equivalent form presented in Eq. (7) and according to the transformed model parameters employed (Table 2), the symmetric offset position for the analytical model is $d = 1$ m. To reflect the small asymmetry in the analytical model for qualitative comparison purposes, a static offset of $d = 1.06$ m is included in the calculation of the analytical results presented in Fig. 5(*b*). Recall that the transformed analytical model parameters are selected with the intention of facilitating a qualitative comparison to experimental results at this phase of the research. In spite of the limitations of the current analytical model parameter selections, the predictions shown in Fig. 5 exemplify good qualitative agreement with the corresponding measurements, revealing distinct low and high amplitude intrawell responses in both potential wells, as well as the higher amplitude snap-through oscillations at low excitation frequencies. This good agreement verifies that the model transformations from the exact formulation in Eq. (4) to the form in Eq. (7) enable a meaningful prediction of the unique dynamic behaviors of the metastable module, and provide a computationally efficient means to analytically predict the steady-state dynamics near resonance. Based on the current results obtained, the derivation of the exact transformed system parameters from Eq. (6) to Eq. (7) may enable a quantitative comparison between the experimental and analytical findings during future studies of this research.

The activation of numerous distinct dynamic responses from the near-resonant excitations suggests that the energy dissipation characteristics are also distinct. To quantify the energy dissipated over one excitation period, the reaction force F as defined in Eq. (5) is plotted against global end displacement Z over one excitation period. Using $W = \int F \cdot \mathrm{d}Z$, the work W done by the reaction force may be calculated over one period of excitation. Since the excitation and response are periodic, the force–displacement trajectory forms a loop. The area enclosed by this loop, resulting from damping-induced hysteresis, is the work done by the reaction force and is equal to the energy dissipated by the module over a single excitation period [19].

The solid curves in Fig. 6(*a*) present the hysteresis loops of a snap-through response obtained from the experimental time-series data using an excitation frequency of 12.5 Hz, and both intrawell responses observed at an excitation frequency of 22 Hz, all using an offset of $D = 0$ mm. These excitation conditions correspond to the angular rotation amplitude data point in Fig. 5(*a*) indicated by the triangle for the snap-through response, and the multiplication and addition symbols for the intrawell #1 and intrawell #2 responses, respectively. The solid curves in Fig. 6(*b*) show the corresponding simulation results obtained by numerically integrating Eq. (4) which is the governing equation of motion for the experimental system. The plots also show dashed curves which are the corresponding static force–displacement profiles. The static profiles are determined by solving Eq. (6) under static conditions and for a fixed global end displacement Z. Similar to the

dashed curve in Fig. 1(*a*), the static force–displacement characteristics for the metastable module studied here demonstrate a range of global end displacements for which two metastable states occur. The snap-through result of Fig. 6(*b*) demonstrates good agreement with the experimental result in Fig. 6(*a*), and shows large reaction force amplitudes having a mean value over the loop which is approximately zero. This suggests that the dynamic reaction force behavior is associated with snap-through since there is no force bias typical of intrawell oscillations. In fact, examinations of the experimental and simulated time-series data (not shown here) confirm that the dynamic responses are correctly identified as snap-through, since the rotating arms oscillate across the central, unstable equilibrium twice per excitation period. Furthermore, the snap-through hysteresis loops display a negative mean slope, indicating the manifestation of negative dynamic stiffness in this regime [19]. The large displacement amplitude of the internal coordinate in the snap-through regime corresponds to large deflections of the linear springs. Due to the more significant internal deformations and the damping present in the module, a large dissipation of energy is achieved for relatively small excitation amplitudes of the global end displacement.

It is clearly seen that each of the intrawell responses in Fig. 6 is confined to a single potential well around a static equilibrium, resulting in a smaller hysteresis loop and consequently much lower energy dissipation per excitation cycle than the snap-through case. The per-cycle energy dissipation predicted by simulation for the intrawell cases in Fig. 6(*b*) is 15.2 μJ, which is much lower than the 54.9 μJ and 61.2 μJ of energy dissipated in the experimental system. This could be due to the unmodeled stick–slip friction in the bearings of the experimental metastable module, which have the effect of increasing damping for low-amplitude oscillations. Thus, there is greater deviation in the values of the area enclosed in the hysteresis loops between the measurements and simulations for the small amplitude intrawell dynamics than for the corresponding measures for the large amplitude snap-through responses.

As seen in Fig. 5, excitation frequency is one factor that determines whether intrawell or snap-through responses are activated. Small changes in frequency may maintain a given response type although the response amplitude and phase may smoothly vary. Consider Fig. 7 which shows experimental and simulated hysteresis loops of snap-through responses as the excitation frequency is varied from 10 Hz to 14 Hz. The area enclosed by the loops, and consequently the energy dissipated per excitation cycle, increases with the increase in frequency. This finding is consistent with results presented in Fig. 5(*a*), which show snap-through response amplitudes increasing with frequency. As the arm rotation angle amplitude increases, the deflection of the linear springs likewise grows in magnitude; consequently, the reaction force amplitude also increases according to Eq. (5). This results in the steady magnification of the hysteresis loops as the frequency increases from 10 to 14 Hz in Fig. 7. Similar to the results of Fig. 6, good overall agreement is seen comparing the experimental results in Fig. 7(*a*) of the snap-through dynamics with the behaviors predicted from the direct simulations of the model governing equations as shown in Fig. 7(*b*).

The results suggest that energy dissipation performance is affected by excitation frequency in the following two ways. First, the excitation frequency influences which dynamic response regimes are realizable. Intrawell and snap-through responses induce particularly different hysteresis loops due to the much larger amplitudes of arm rotation triggered by the snap-through behaviors. Thus, large adaptation of energy dissipation (orders of magnitude) may be accomplished. Second, small changes in excitation frequency that maintain a particular response regime may have a lesser, but still appreciable, effect on the energy dissipated

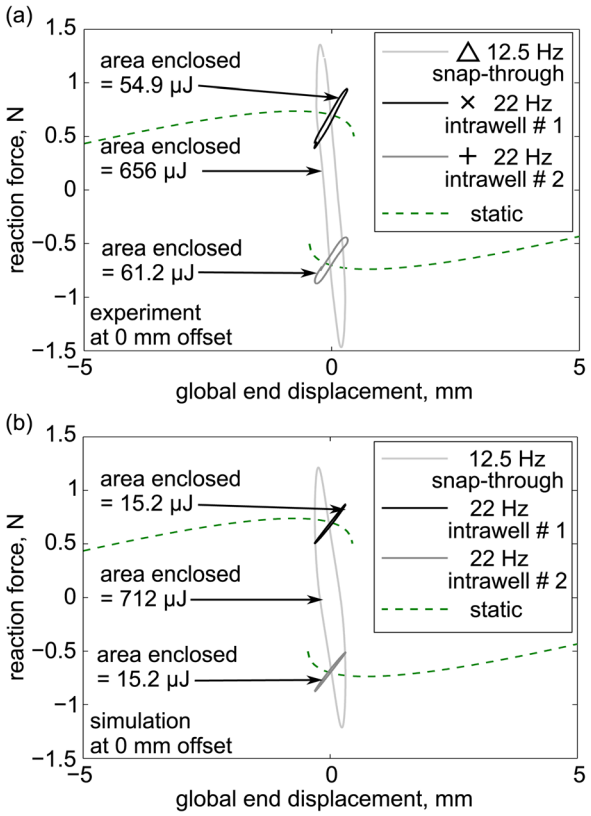

Fig. 6 (*a*) Experimental and (*b*) simulated hysteresis loops (solid curve) of a snap-through response at 12.5 Hz excitation, and an intrawell response at 22 Hz excitation with 0 mm offset. Symbols in the legend of (*a*) correspond to the respective conditions from Fig. 5(*a*).

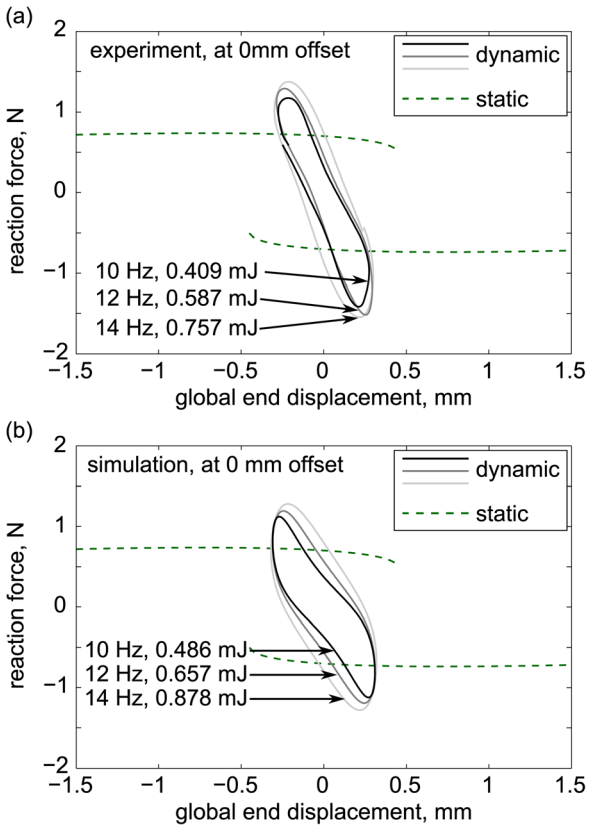

Fig. 7 (*a*) Experimental and (*b*) simulated hysteresis loops (solid curves) of snap-through response at 0 mm offset at different excitation frequencies

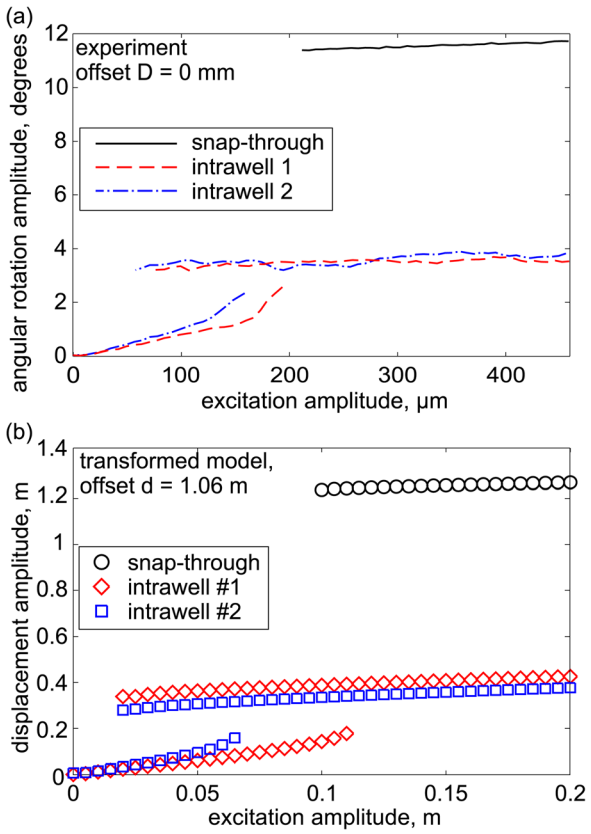

Fig. 8 (*a*) Experimental and (*b*) analytical results of the influence of excitation amplitude on the internal dynamics of the metastable module when excited at constant frequency

per cycle. In this way, a refined modulation of the energy dissipation may be induced.

6 Excitation Level Influence on Energy Dissipation

Excitation level is shown to have a strong influence on the dynamic behavior of bistable oscillators [6,20] and is expected to exert similarly strong influence on the metastable module which contains a bistable element. To study the influences, several excitation amplitude sweeps are performed at fixed excitation frequencies. Figure 8(*a*) presents the experimental results of an excitation amplitude sweep from 0 to 450 μm at a rate of 2.25 μm/s, with constant excitation frequency $\Omega/2\pi = 17$ Hz. Figure 8(*b*) shows analytical model results, computed using an excitation frequency $\omega/2\pi = 5.03$ Hz and with the model parameters given in Table 2. Similar to the good agreement seen in Fig. 5, the comparisons in Fig. 8 indicate that the analytical model provides a meaningful prediction of the qualitative behaviors observed experimentally when the excitation amplitude is varied while the excitation frequency remains constant. Both the experimental and analytical results show the presence of low amplitude intrawell oscillations only at low excitation levels, and a range for which low and high amplitude intrawell responses coexist. Snap-through responses are observed at high excitation amplitudes. The high amplitude intrawell and the snap-through regimes show fairly constant response amplitudes over a large range of excitation amplitudes, indicating robustness to changes in excitation level.

Figure 8 indicates that the existence or coexistence of dynamic response regimes is strongly influenced by excitation amplitude. To demonstrate how these trends correspond to energy dissipation performance, Figs. 9(*a*), 9(*b*), and 9(*c*) show hysteresis loops at 200 μm, 300 μm, and 450 μm excitation amplitudes, respectively, for a fixed 17 Hz excitation frequency, and offset $D = 0$ mm. It is observed that as excitation amplitude is increased, the amount of energy dissipated in a particular response regime is slightly increased, consistent with the results presented in Fig. 8(*a*).

Thus, the excitation amplitude influences the energy dissipation characteristics in ways comparable to excitation frequency. First, excitation amplitude affects the dynamic response regimes that are realizable, where each regime results in different energy dissipation. At very low excitation levels, only low amplitude intrawell responses are observed. As excitation level increases, the low amplitude intrawell responses vanish while high amplitude intrawell and snap-through responses are activated. Second, increased excitation amplitude increases the amount of energy dissipated per excitation cycle for a fixed response regime. This is a desirable characteristic in practice, where greater excitation levels typically call for increased damping and energy dissipation performance.

7 Offset Influence on Energy Dissipation

Thus far, the studies have focused on excitations that are ideally symmetric about the unstable equilibrium position of the internal bistable element of the metastable module. Yet, once the excitation is applied with an offset from the symmetric condition, asymmetry may appear in the dynamic response, since the bistable constituent of the metastable module is under an additional static force ($K_L D$). In practice, such a load may be representative of a mass supported by the module under gravitational body forces.

The influences upon the steady-state dynamics of the module due to a static offset D that modulates the symmetry of the system are examined in Figs. 10 and 11 for a fixed excitation amplitude of $Z_0 = 300$ μm in the experiments and $z_0 = 0.1$ m in the analytical model. Figure 10(*a*) presents experimental results where the excitation offset D is 0.7 mm deflected from the neutral position, while Fig. 10(*b*) shows qualitatively similar analytical results for the offset of $d = 1.2$ m. The offset biases the metastable module toward well #1; the dynamics of this state are shown using dashed curves and diamonds in Figs. 10(*a*) and 10(*b*), respectively. The asymmetry results in a greater bandwidth of frequencies for which

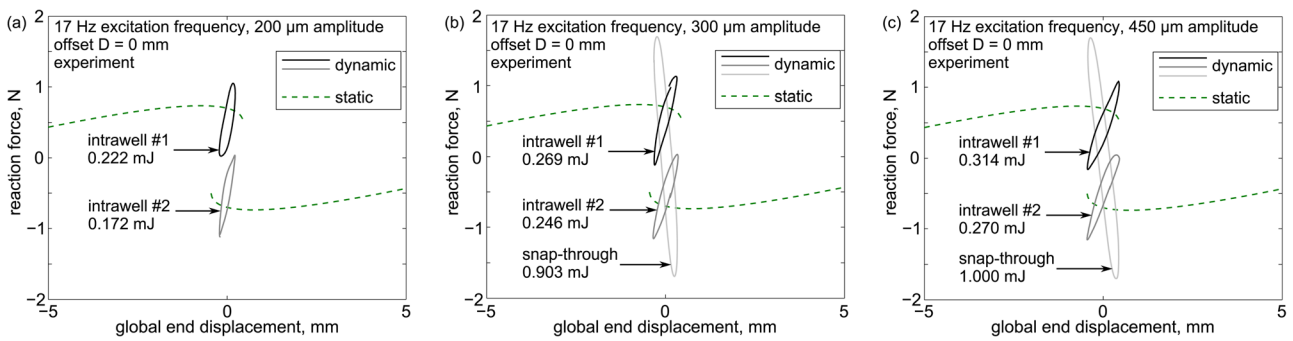

Fig. 9 Experimental hysteresis loops (solid curves) at $D = 0$ mm offset, 17 Hz excitation frequency, and (*a*) 200 μm, (*b*) 300 μm, and (*c*) 450 μm excitation amplitude. Response type and area enclosed by each loop are indicated.

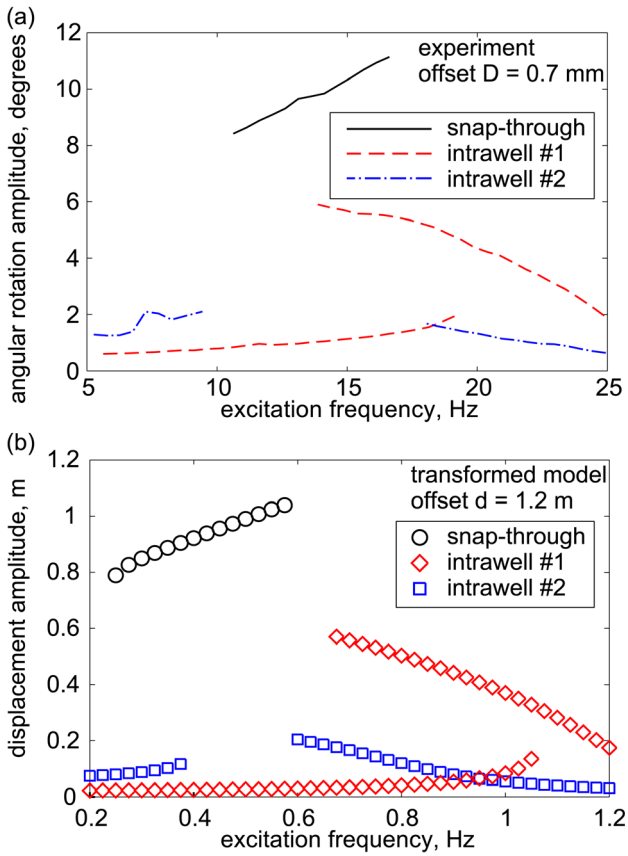

Fig. 10 (*a*) Experimental and (*b*) analytical results showing the internal dynamics of the metastable module as excitation frequency is varied, while the excitation amplitude and offset remain fixed

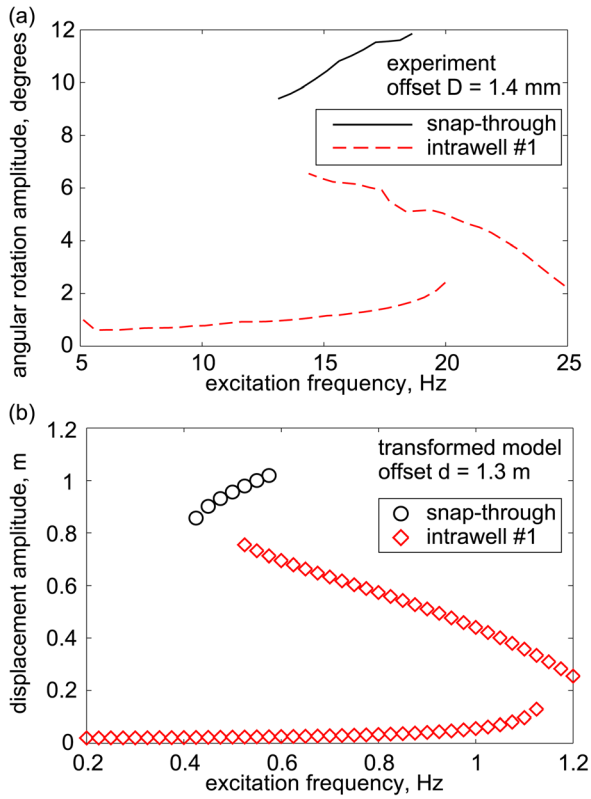

Fig. 11 (*a*) Experimental and (*b*) analytical results showing the internal dynamics of the metastable module as excitation frequency is varied, while the excitation amplitude and offset remain fixed. A greater offset is used than that employed for the results shown in Fig. 10.

the steady-state intrawell responses occur when the internal mass is confined to well #1, whereas the frequency range of existence for motions in well #2 is greatly diminished (dashed–dotted curves and squares in Figs. 10(*a*) and 10(*b*), respectively). Qualitatively, the change in offset plays a key role in tailoring the local linearized resonant frequencies of the intrawell behaviors, and thus governs the frequency bandwidths across which each set of low and high amplitude intrawell dynamics may occur. As a result, the energy dissipation characteristics of these regimes are strongly controlled via offset modulation.

Additionally, in comparing the experimental and analytical results from Fig. 5 to those in Fig. 10, the frequency bandwidth for which snap-through motions are observed is modulated. In other words, the offset has the effect of tailoring the bandwidth of frequencies for which the large dissipation capability of the snap-through dynamics is realized. The asymmetry introduced by the static offset also results in intrawell #1 and #2 responses exhibiting notably different response amplitudes for the same excitation frequency. Collectively, the results show that application of an offset to the harmonic excitation of the metastable module leads to a versatile range of energy dissipation performance according to the operating frequency and amplitude of the induced dynamics of the internal bistable element.

When the offset is further increased to $D = 1.4$ mm in the experiment, as shown in Fig. 11(*a*), well #2 is no longer statically stable, and no steady-state intrawell responses are found in well #2 at any frequency. Analytical results in Fig. 11(*b*) with an offset of $d = 1.3$ m demonstrate comparable behavior. Compared to Fig. 10, the size of the frequency bandwidth for which the same type of intrawell responses in well #1 exist is further increased. However, the absence of stable intrawell responses in well #2 means that fewer frequencies exhibit multiple coexistent responses regimes, compromising some energy dissipation adaptability. Considering the snap-through responses from Figs. 5 to 10 to 11, it is apparent that change in the excitation offset from a near-symmetric excitation condition has the effect of modulating the bandwidth of frequencies for which the snap-through motions occur. In particular, an increase of the offset increases the lower and upper frequency extents of the bandwidth although the total bandwidth is seen to remain relatively constant. This finding suggests that a novel bandpass filter feature may be realized for the metastable module in terms of triggering large damping associated with the snap-through behaviors for a particular range of excitation frequencies.

While the introduction of a nonzero static offset to the excitation affects the frequency ranges in which the different response regimes are observed, certain excitation frequencies exhibit the same response regime at all three offsets $D = 0$ mm, 0.7 mm, and 1.4 mm, permitting an analysis of the impact of offset on energy dissipation performance. To examine one example, Fig. 12 presents measured hysteresis loops for snap-through responses when excited at 14 Hz. As the offset is increased (shown by the increasing lightness of the solid curves), the centers of the hysteresis loops move toward the statically stable well, although the amount of energy dissipated per cycle varies only slightly. This indicates that the energy dissipation performance in the snap-through regime is robust to small changes in excitation offset. This result is useful for applications in which high energy dissipation is desired but equivalent offset influences vary over time, such as change in applied dead loads or supported weights.

As evidenced by the frequency sweep results presented in Figs. 10 and 11, excitation offset may affect which response regimes are physically realizable. The experimental results in Fig. 10(*a*) suggest that low and high amplitude intrawell and snap-through responses may be observed for excitation frequencies

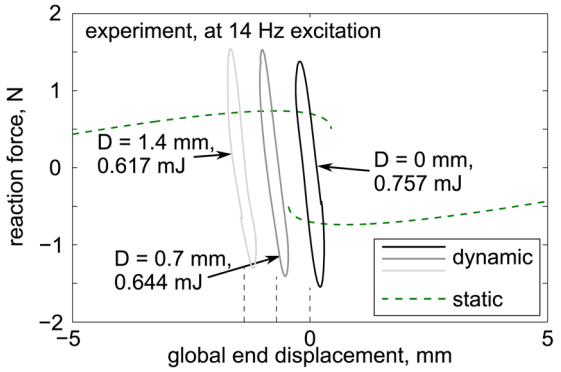

Fig. 12 (*a*) Experimental hysteresis loops (solid curves) for snap-through responses at 14 Hz excitation. Excitation offset and area enclosed by each loop are indicated.

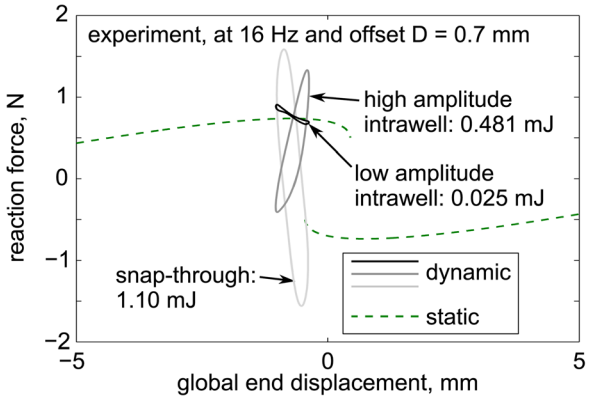

Fig. 13 (*a*) Experimental hysteresis loops (solid curves) at 16 Hz excitation and $D = 0.7$ mm offset. Response type and area enclosed by each loop are indicated.

between about 14 Hz and 17 Hz with an offset $D = 0.7$ mm. Figure 13 presents hysteresis loops for the three coexistent responses at 16 Hz excitation frequency. There is a 44 times difference in energy dissipation from the low amplitude intrawell to the snap-through responses, while the high amplitude intrawell dynamics provide an intermediate level to bridge the extremes. This exemplifies the significant adaptation of energy dissipation enabled by the metastable module for fixed excitation parameters by switching among the various dynamic states, for example via strategic perturbations or different initial conditions. In fact, with appropriate design the module may exhibit five coexistent dynamic responses: low and high amplitude intrawell oscillations in each potential well, along with snap-through.

8 Conclusion

This paper explores the unique dynamic and energy dissipation characteristics of a metastable module excited at frequencies near resonance. An archetypal metastable module, representing a fundamental unit for the integration of negative stiffness bistable elements within an overall structural system, is designed, fabricated, and modeled. Although the module contains a bistable constituent, the static and dynamic properties of the metastable module are significantly distinct when compared to the properties of an individual bistable element. The prescribed amplitude and frequency of harmonic global end displacement excitations on the metastable module are found to affect the existence or coexistence of multiple dynamic regimes that display an order of magnitude of difference in energy dissipation amongst them. Tailoring the displacement offset presents another method to modify energy dissipation characteristics, due to asymmetric static mechanical properties that govern the realization of particular dynamic energy dissipation regimes. These characteristics may be used to develop vibration damping devices having large and adaptable energy dissipation properties for applications with diverse and demanding performance needs.

Acknowledgment

This research was supported by the Air Force Office of Scientific Research (FA9550-13-1-0122) under the administration of Dr. David Stargel and by the University of Michigan Collegiate Professorship.

References

[1] Lakes, R. S., 2001, "Extreme Damping in Compliant Composites With a Negative-Stiffness Phase," Philos. Mag. Lett., **81**(2), pp. 95–100.
[2] Wang, Y. C., and Lakes, R. S., 2005, "Composites With Inclusions of Negative Bulk Modulus: Extreme Damping and Negative Poisson's Ratio," J. Compos. Mater., **39**(18), pp. 1645–1657.
[3] Klatt, T., and Haberman, M. R., 2013, "A Nonlinear Negative Stiffness Metamaterial Unit Cell and Small-on-Large Multiscale Material Model," J. Appl. Phys., **114**(3), p. 033503.
[4] Kochmann, D. M., 2014, "Stable Extreme Damping in Viscoelastic Two-Phase Composites With Non-Positive-Definite Phases Close to the Loss of Stability," Mech. Res. Commun., **58**, pp. 36–45.
[5] Barbarino, S., Pontecorvo, M. E., and Gandhi, F. S., 2012, "Energy Dissipation of a Bi-Stable von-Mises Truss Under Harmonic Excitation," AIAA Paper No. 2012-1712.
[6] Johnson, D. R., Thota, M., Semperlotti, F., and Wang, K. W., 2013, "On Achieving High and Adaptable Damping Via a Bistable Oscillator," Smart Mater. Struct., **22**(11), p. 115027.
[7] Kashdan, L., Seepersad, C. C., Haberman, M., and Wilson, P. S., 2012, "Design, Fabrication, and Evaluation of Negative Stiffness Elements Using SLS," Rapid Prototyping J., **18**(3), pp. 194–200.
[8] Fulcher, B. A., Shahan, D. W., Haberman, M. R., Seepersad, C. C., and Wilson, P. S., 2014, "Analytical and Experimental Investigation of Buckled Beams as Negative Stiffness Elements for Passive Vibration Isolation and Shock Isolation Systems," ASME J. Vib. Acoust., **136**(3), p. 031009.
[9] Dong, L., and Lakes, R. S., 2013, "Advanced Damper With High Stiffness and High Hysteresis Damping Based on Negative Structural Stiffness," Int. J. Solids Struct., **50**(14–15), pp. 2416–2423.
[10] Nadkarni, N., Daraio, C., and Kochmann, D. M., 2014, "Dynamics of Periodic Mechanical Structures Containing Bistable Elastic Elements: From Elastic to Solitary Wave Propagation," Phys. Rev. E, **90**(2), p. 023204.
[11] Cohen, T., and Givli, S., 2014, "Dynamics of a Discrete Chain of Bi-Stable Elements: A Biomimetic Shock Absorbing Mechanism," J. Mech. Phys. Solids, **64**, pp. 426–439.
[12] Lakes, R. S., and Drugan, W. J., 2002, "Dramatically Stiffer Elastic Composite Materials Due to a Negative Stiffness Phase?" J. Mech. Phys. Solids, **50**(5), pp. 979–1009.
[13] Bažant, Z. P., and Cedolin, L., 2010, *Stability of Structures: Elastic, Inelastic, Fracture, and Damage Theories*, World Scientific Publishing, Hackensack, NJ.
[14] Virgin, L. N., 2007, *Vibration of Axially Loaded Structures*, Cambridge University Press, Cambridge, UK.
[15] Rao, S. S., 2004, *Mechanical Vibrations*, 4th ed., Pearson Prentice Hall, Upper Saddle River, NJ.
[16] Kovacic, I., and Brennan, M. J., 2011, *The Duffing Equation: Nonlinear Oscillators and Their Behaviour*, Wiley, New York.
[17] Nayfeh, A. H., and Mook, D. T., 1995, *Nonlinear Oscillations*, Wiley, Weinheim, Germany.
[18] Harne, R. L., Thota, M., and Wang, K. W., 2013, "Concise and High-Fidelity Predictive Criteria for Maximizing Performance and Robustness of Bistable Energy Harvesters," Appl. Phys. Lett., **102**(5), p. 053903.
[19] Lakes, R. S., 2009, *Viscoelastic Materials*, Cambridge University Press, Cambridge, UK.
[20] Wiebe, R., Virgin, L. N., Stanciulescu, I., Spottswood, S. M., and Eason, T. G., 2012, "Characterizing Dynamic Transitions Associated With Snap-Through: A Discrete System," J. Comput. Nonlinear Dyn., **8**(1), p. 011010.